PCCP

Accepted Manuscript

ROYAL SOCIETY OF CHEMISTRY

www.rsc.org/pccp

A Size Dependent Discontinuous Decay Rate for the Exciton Emission in ZnO Quantum Dots

T. Jesper Jacobsson[1]*, Sviatlana Viarbitskaya[2], Emad Mukhtar[1] and Tomas Edvinsson[1]

1) Department of Chemistry - Ångström Laboratry, Uppsala University, Box 538, 75121 Uppsala, Sweden
2) Laboratoire Interdisciplinaire Carnot de Bourgogne CNRS-UMR 6303, Université de Bourgogne, 21078 Dijon, France

Jesper.jacobsson@kemi.uu.se, +46 (0)70-5745116

Abstract

The time resolved UV-fluorescence in ZnO quantum dots have been investigated with femtosecond laser spectroscopy. The measurements were performed as a function of particle size for particles between 3 and 7 nm in diameter, which are in the quantum confined regime. A red shift in the fluorescence maximum is seen while increasing the particle size, which correlates with the shift in band gap due to quantum confinement. The energy difference between the UV-fluorescence and the band gap does, however, increase for the smaller particles. For 3.7 nm particles the fluorescence energy is 100 meV smaller than the band gap energy, whereas it is only 20 meV smaller for the largest particles. This indicates a stabilization of the excitons in the smallest particles. The lifetime of the UV fluorescence is in the picosecond time scale and interestingly, it is discontinuous with respect to particle size. For the smallest particles, the exciton emission life time reaches 30 ps, which is three times longer than for the largest particles. This demonstrates a transition between two different mechanisms for the UV-fluorescence. We suggest that this is an effect of surface trapping and stabilization of the excitons occurring in the smallest particles but not in the larger ones. We also discuss the time scale limit for slowed hot carrier dynamics in ensembles of quantum confined ZnO particles.

1. Introduction

Zinc oxide is a familiar and commonly used substance. More than 10^5 tons of bulk ZnO are produced annually[1], and ZnO have been used in technological applications for centuries. ZnO is found in everyday products, like for example: sunscreens[2], pigments[3], food additives[4] and rubber[5]. Besides from these conventional applications, ZnO, and especially various nanoscale morphologies, has emerged as a promising material for a large set of new high tech applications. Among these are: UV-lasers[6], light emitting diodes[7], field emitters[8], piezo-electric devices[9], spintronic devices[10], gas sensors[11], transparent conductors[12], self-powered nanosystems[13], monetary surveillance[14], photovoltaics[15] and photocatalysis[16] to mention just a few.

Several of these applications are based on the optical properties of ZnO. Some are rather straightforward, like UV-absorption in sun screens and light scattering in pigments. Others are more elaborate and depend on luminescence and fluorescence, which are more difficult to understand and to control. ZnO have a band gap of around 3.3 eV and a large exciton binding energy of 60 meV[17], resulting in bright room temperature emission. This together with rich defect chemistry opens up for the broad and varied landscape of interesting fluorescence behavior which is the scope of this work.

A lot of attention has been directed towards fluorescence in ZnO due to the potential applications in for example light emitting devices, and a number of reviews are found in the literature[1,18]. A common claim in these reviews is that so far, there is no consensus over the exact mechanism behind the different modes of fluorescence found in ZnO.

ZnO is often ascribed two different modes of fluorescence emission; one in the UV region and one in the visible with a yellow/green color. Emissions have, however, been experimentally reported over more or less the entire visible spectra, with for example both blue[19] and orange fluorescence[20]. Some work also indicate that the fluorescence, under certain conditions, can be tuned over a wide spectrum[14,21-23]. Several different hypotheses for the precise mechanisms for these transitions have been suggested. It is, however, clear that defects, both intrinsic and caused by intentional or unintentional doping, are vital for the fluorescence behavior. Much evidence also points to the importance of grain boundaries and surface properties. In a previous paper, we have investigated the yellow/green fluorescence in wurtzite ZnO as a function of particle size[24]. We have also developed a method for pinpointing the absolute energetic positions of the trap levels involved in that fluorescence, which were applied on particles on different sizes[25].

The focus of this work is instead on the kinetics and mechanisms behind the UV-fluorescence, which is investigated using femtosecond laser spectroscopy. The measurements are performed as a function of particles size for particles in the quantum confined regime with diameters between 3 and 7 nm. The UV-fluorescence is less studied than the visible counterpart; in part because it has been conjectured to have a simpler mechanistic origin. It has been ascribed to band gap or exciton recombination, and is known as a substantially faster process than the visible fluorescence[26]. Here we demonstrate the mechanism to be far from trivial and how increased knowledge of the energetics and kinetics of this transition can help in understanding the dynamics of the interaction with light and ZnO nanostructures. Evidence is found for two different mechanisms, with different kinetics, for the UV-fluorescence. We further demonstrate a discontinuous transition between the two mechanisms with respect to particle size, where the emission has a longer lifetime for the smaller particles. Information is also extracted concerning hot carrier relaxation and the coupling between the mechanism for the UV and visible emission in ensembles of quantum dots. These results should be of importance in the design of advanced ZnO based devices.

2. Methods

2.1 Synthesis

ZnO nanoparticles were synthesized by a wet chemical method based on hydrolysis in alkaline zinc acetate solution. The synthesis is based on work of Meulekamp[27] and Spanhel et al.[28] and were described in more detail in a previous publication[24]. In short, 2.5 mmol $Zn(OAc)_2 \cdot 2\ H_2O$ was dissolved in 25 ml boiling ethanol, under vigorous stirring, for approximately one minute. The solution was subsequently cooled to room temperature and mixed with 3.5 mmol $LiOH \cdot H_2O$ dissolved in 25 ml ethanol. When the two solutions were mixed, ZnO quantum dots begin to nucleate and grow, which can be monitored by measuring the change in band gap with UV-vis spectroscopy[24,29]. At certain times, a small volume of solution was used in order to make films of particles with distinct sizes. 2.5 ml of the reaction solution were then mixed with approximately 5 ml hexane, which induces particle agglomeration and precipitation. In order to increase the speed of the sedimentation, the solution was centrifuged at 5000 rpm for five minutes. The particles were then redispersed in one drop of methanol and ultrasonicated for 3 minutes, after which smooth, transparent thin films were deposited by doctor blading. Fluorine doped SnO_2 (FTO), Pilkinton TEC 8, were used as substrates for film deposition. The transparent conducting substrates were used in order to enable combined electrochemical and transient absorption measurements.

2.2 Measurements and characterization

The UV-vis absorption measurements were performed on an Ocean Optics HR-2000+ spectrophotometer with deuterium and halogen lamps. In all measurements, a full spectrum from 190 to 1100 nm with 2048 evenly distributed points was sampled. In order to obtain good statistics, an average over 100 consecutive spectra were performed.

XRD measurements were performed with a Siemens D5000 Diffractometer, using parallel beam geometry, an x-ray mirror and a parallel plate collimator of 0.4°. $Cu_{k\alpha}$ with a wavelength of 1.54 Å was used as x-ray source. The angle of incidence was 0.5° and 2Θ scans were performed between 10° and 90° using a step size of 0.1°.

The excitation source used for the time resolved fluorescence measurements was a 200 kHz femtosecond laser amplifier system (Coherent), operating at 790 nm. The system consists of an 18 W diode pumped, frequency double Nd:YLF laser (526 nm) which is used as a pump source for a Ti:Sapphire mode locked laser (Mira). The latter seeds a Ti–Sapphire regenerative amplifier (RegA 9000). The amplifier produces pulses of approximately 1 W at 200 kHz. The pulse width was 120 fs as determined by the autocorrelation trace. The output of the amplifier was then used to pump an optical parametric amplifier (Coherent: OPA). The OPA was tuned to 640 nm which was then frequency doubled to 320 nm for sample excitation.

The sample was excited at 45º incident angle and the emitted fluorescence was measured using a Hamamatsu streak camera. The fluorescence was collected at right angle to the excitation and was passed through a Bruker SPEC 250IS spectrograph (200 nm observation window) and onto the streak camera and blanking unit (C5680) in combination with a Synchroscan Unit (M5675). The charge-coupled device (CCD) camera (Hamamatsu Orca-ER C4742−95) was used in binning mode (2 × 2 pixels) to give a 512 × 512 pixel matrix. The observation window was in the time-ranges of 800 ps, giving an instrument response function (FWHM) of approximately 20 ps.

3. Theory

ZnO is known to show fluorescence in both the visible and in the ultraviolet region. The mechanisms for these different modes of fluorescence tend to be coupled in the sense that if the magnitude of one is increased, it is at the expense of the other[18,30,31]. The experimental focus of this paper is on the UV-fluorescence, but to present the complete picture, the visible fluorescence is shortly reviewed. The green fluorescence for these particles has been investigated in some detail in previous publications[24,25]. The magnitude of the visible fluoresces was demonstrated to be linked to the total amount of particle surface in the system, as well as to the nature of these surfaces. The fluorescence energy is blue shifted with decreased particle size in line with the corresponding shift of the band gap energy. The visible fluorescence were further found to be caused by a transition between trap states located approximately 0.35 eV below the conduction band edge, down to deep traps in the band gap[25]. The energy shift between the conduction band edge and the upper trap levels is independent of particle size. A summary of this behavior is given in figure 1.a and are more thoroughly discussed in our earlier publications[24,25]. The correlation between the visible fluorescence and the UV-fluorescence will be discussed further in the result section.

An area where time resolved UV-fluorescence measurements can give important information is the nature of the hot carrier dynamics. A major loss mechanism in solar cells, photo catalysts and other light harvesting devices is the thermalization of photogenerated charge carries, where the hot carriers are losing their excess kinetic energy, E_k, by interaction with phonons. An illustration of possible pathways related to hot carriers is given in figure 1.b. It would be highly beneficial if the thermalization could be avoided, or slowed down enough for the charge carriers to be utilized while still in their hot state. Solar cells with higher theoretical efficiencies, far surpassing the well-known Shockley-Queisser limit, and photo catalyst utilizing a higher overpotential could then in principle be assembled. It has therefore been a hot topic in the literature[32-34]. For most structures, thermalization is a process in the sub picosecond time range, but for quantum wells and quantum dots it has been suggested, and also experimental verified, that it could be slowed down[32,35]. This is a consequence of a phonon-bottleneck[36], which basically is a reduced coupling between the charge carriers and a non-equilibrium phonon distribution. This in turn is a consequence of the increased spread in energy levels due to quantum confinement.

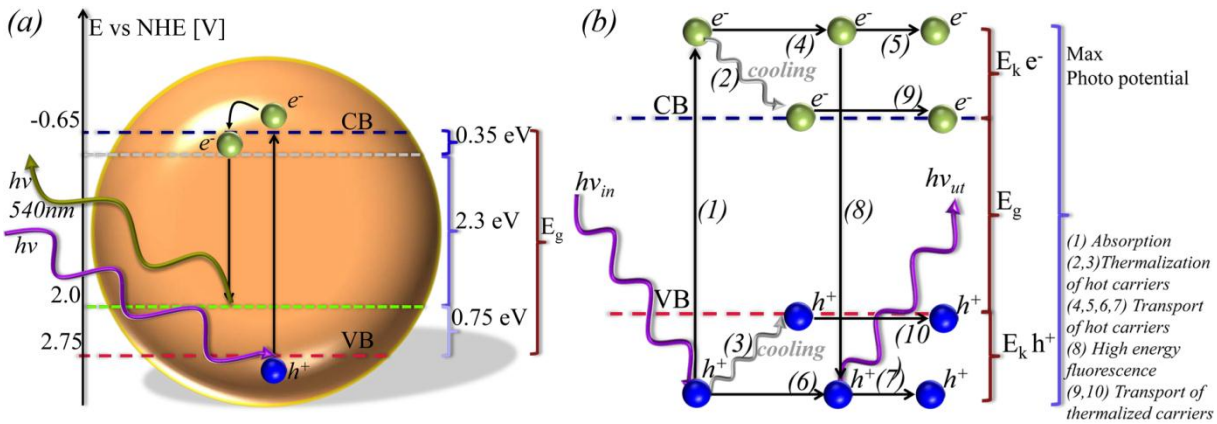

Figure 1. (a) Graphical summary of the energetics of the visible fluorescence previously measured for the same particles. (b) Illustration of possible pathways for photogenerated electrons and holes in a semiconductor with hot carriers.

An experimental indication of a suppressed phonon cooling can be obtained by measuring the time response of the UV-fluorescence after a laser pulse. In case of slow thermalization, the energy range of the fluorescence would be broader and also spread out to energies larger than the band gap energy (8). This have been observed in for example quantum wells of $GaAs/Al_{0.38}Ga_{0.62}As$[32, 35].

In the case of ZnO quantum dots, both experimental Raman data as well as molecular dynamics simulation show that phonons are suppressed in particles in the size regime used in this study[37]. This suggests that ZnO quantum dots could be a possible candidate material for hot carrier applications, well worth investigating with this in mind. The most interesting morphology for these applications are particles deposited as thin films on conductive substrates. The proximity between particles in dense films increases the risk of rapid thermalization and charge transfer induced quenching compared to isolated single particles. As hot carriers cannot be utilized unless extracted through an ensemble of particles, dense films are, however, the most relevant systems to investigate in this context.

4. Results

An X-ray diffractogram of a representative ZnO sample is given in figure 2.a. From the figure it is evident that the particles are ZnO of wurtzite structure[38] and that no other crystalline phases are present. Also evident is the peak broadening caused by the small size of the particles. A more extensive analysis of these particles with XRD[24], UV-Vis absorption[29] and Raman spectroscopy[37] are found in our previous papers. For a more in-depth material characterization and a discussion concerning particle shape, structure and polydipersity, the reader is referred to those articles.

In this study, 8 samples in the form of thin films with different quantum dot sizes between 3.7 and 6.3 nm were analyzed. Optical absorption for these samples is found in figure 2.b, from which the optical band gaps can be extracted by plotting the square of the measured absorption and extrapolating the linear region, for photon energies slightly higher than the band gap, down to zero absorption as in figure 2.c. For these small particles, the band gap increase monotonically with decreased particle size, and by knowledge of the relation between the two parameters the volume average particle diameters can be extracted as described in the references[24]. The particle diameters of the samples investigated are given in the legend of figure 2.b and are below 7 nm, which for wurtzite ZnO are in the domain of electronic quantum confinement.

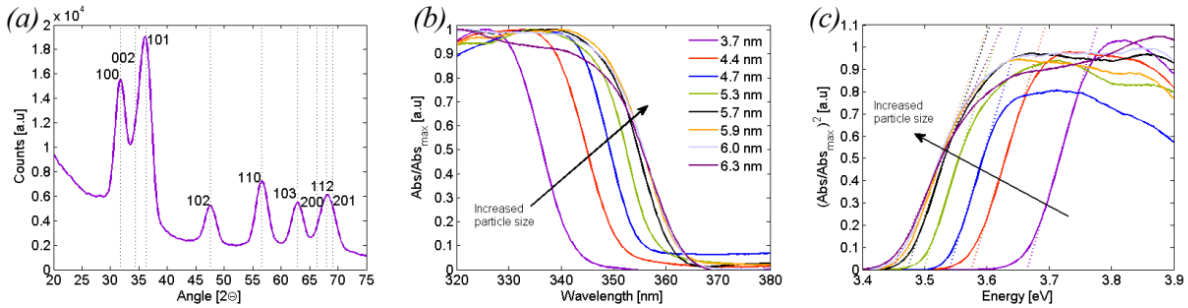

Figure 2. (a) XRD data for 6 nm particles. The vertical lines represent literature data for wurtzite ZnO. (b) Normalized absorption data for the analyzed samples. (c) Determination of the band gap as the intercept between the photon energy and the extrapolation of the linear region of the square of the absorption.

For the femtosecond spectroscopy, an excitation wavelength of 320 nm and a 120 fs laser pulse were used and the emission response was measured between 274 and 545 nm in the

picosecond regime in a time interval of 793 ps. The contour plot for the response for the 4.7 nm particles is given in figure 3.a. Plots for the entire dataset are found in the supporting information. The time scale in figure 3 is defined so that time zero coincides with the time for the peak of the laser-pulse seen at 320 nm. The fluorescence is seen as a weaker signal around 350-360 nm. To improve the readability, the UV-fluorescence is cut out and represented as a 3D-suface in figure 3.b, showing a decay rate in the low picosecond regime. Another interesting feature is an asymmetry in the signal with respect to wavelength, where a tail is stretching out towards longer wavelengths. By normalizing the fluorescence data in figure 3.b for each wavelength, the decay rate for emission of different wavelength can be compared directly. This is done in figure 3.c, where the decay rate is shown to be rather independent with respect to emission wavelength. To get a readable signal in figure 3, the background is removed.

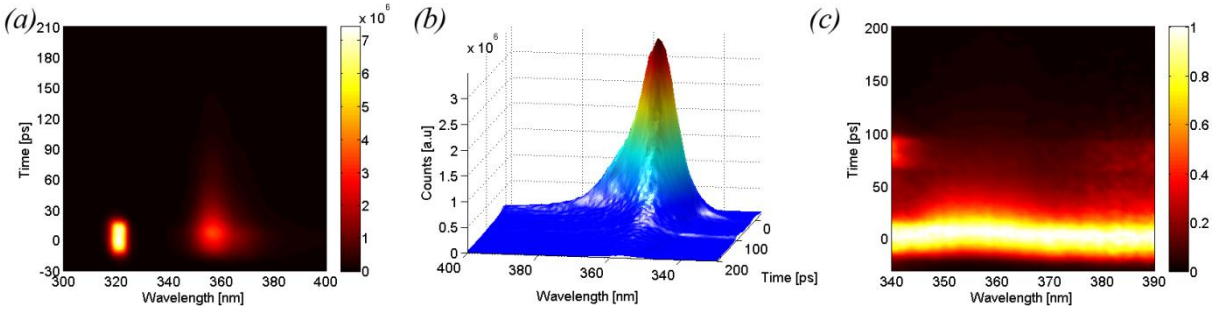

Figure 3. Fluorescence data for the 4.7 nm sample. (a) Contour plot of the response to the 320 nm excitation as a function of wavelength and time. The laser pulse is seen at 320 nm and the fluorescence at longer wavelengths, centered at 357 nm. (b) 3D surface of the fluorescence signal as a function of wavelength and time. (c) Fluorescence response normalized with respect to the peak value for each wavelength as a function of time and wavelength.

By integration along the time axis in figure 3.a, a pure wavelength response is obtain which is given for the 4.7 nm sample in figure 4.a and for the full sample set in figure 4.b. As seen in the figure, the laser signal and the fluorescence are well separated in the wavelength dimension. There is, however, a substantial overlap in the time dimension due to the fast kinetics of the decay and the picosecond response time of the detector. The absolute response in figure 4.b is different for the different samples, which is caused by small variations in the sample alignment. The absolute intensities can therefore not be compared directly for the different samples, and normalized data are therefore used in subsequent comparisons. This, unfortunately, also means that quantum yields are not available with this experimental setup.

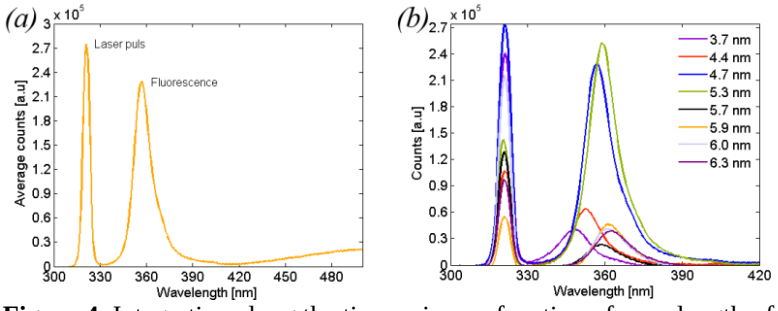

Figure 4. Integration along the time axis as a function of wavelength of the data in figure 3.a. (a) For the 4.7 nm sample. (b) For the full set of samples. The signal seen at longer wavelength in (a) is likely due to noise, background signal or a tail for fluorescence at longer wavelength and should not be of importance for the present analysis.

While the particle size increases, the UV-fluorescence is red shifted analogous to the behavior of the band gap energy and the green fluorescence[24]. This is seen in figure 5.a, where the fluorescence peak is compared for the different samples. This is a consequence of the electronic quantum confinement and the increased cluster like orbitals in the smaller particles. The fluorescence energy is compared with the band gap energy in figure 5.b, showing that the fluorescence energy is somewhat lower than the band gap energy, which in turn is lower than the excitation energy. This energy difference increases with decreased particle size as seen in figure 5.c. For the smallest particles investigated (3.7 nm), the energy difference is in the order of 100 meV and decreases to around 20 meV for particles larger than 5.5 nm in diameter. This could be compared to the ZnO exciton binding energy, commonly reported to be approximately 60 meV[17]. For the smaller particles in the sample set, the UV-fluorescence could therefore be caused by a transition from an exciton state down to the valence band edge. For the larger particles, where the energy difference between the fluorescence and the band gap is smaller than the exciton binding energy, the transition may instead occur directly between the bottom of the conduction band to the top of the valence band.

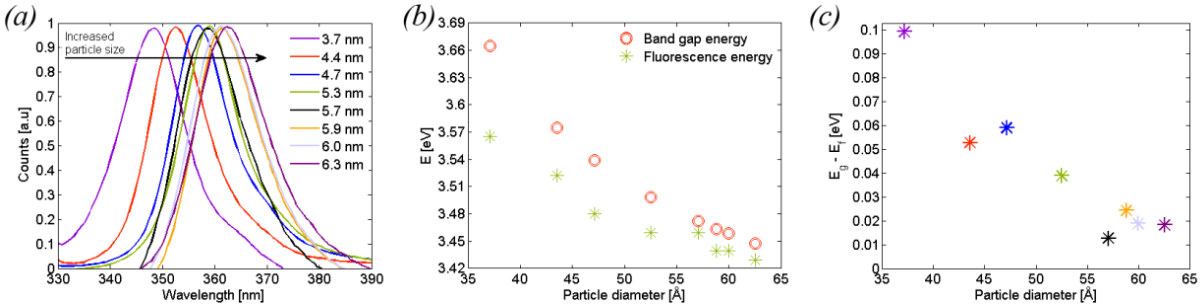

Figure 5. (a) Shift in the fluorescence peak with respect to particle size. (b) Comparison between band gap energy and fluorescence energy as a function of particle size. (c) Difference between band gap energy and fluorescence energy as a function of particle size.

To obtain the kinetic parameters of the UV-decay, the signal is extracted as a function of time for the wavelength where the peak value is recorded. That represents a vertical cut in figure 3.a at 357 nm and will, according to figure 3.b, give representative data for the kinetics of the process. This time track is given for the full sample set in figure 6.a. The decay kinetics is different for the smallest and the largest particles, with a sharp transition between 5.3 and 5.7 nm. The data do not show a smooth continuous transition, but instead one slower decay rate for the smaller particles and a faster decay rate or the larger set of particles. Within the two groups, the decay rates are rather uniform.

The decay rates for both groups of particles are fast with respect to the resolution of the detector system in the measurement, and the laser pulse response show a substantial overlap with the fluorescence in the time dimensions, as illustrated in figure 6.b. The fluorescence decay is comparable, but distinguishable, to the instrumental response function (IRF) of the system, given by the response of the measuring system to the excitation laser pulse at 320 nm. This makes an accurate determination of time constants somewhat more difficult, especially for the larger particles. The existence of a qualitative difference between the two groups of emission lifetime is, however, evident. In order to extract the time constants, τ, the data were analyzed with time deconvolution. The laser pulse was assumed to be Gaussian with respect to time and convoluted with the single exponential decay function in eqn. 1, where I is fluorescence intensity and I_0 the fluorescence intensity at time, t, zero. In this way the experimental data could be fitted with a different contribution from the laser within the Gaussian pulse and the corresponding time constants could be extracted.

$$I(t) = I_0 e^{-t/\tau} \quad (1)$$

The deconvolution procedure was performed using a self-written routine in IgorPro6. In the analysis, the IRF was an adjustable parameter varying between 24-26 ps and a time shift parameter was introduced to account for the wavelength dependence in the measuring system. An illustration of how the model fits the experimental data is given for one sample with larger particles and one with smaller particles in figure 6.c. The values of the time constants are given together with other key data in table 1. The analysis gives a lifetime of approximately 28 ps for the smaller particles and 11 ps for the larger particles, where the exact value of the fastest lifetime is in the region of the detector response time and could also be faster. The distinct separation of the lifetime indicates the existence of at least two different mechanisms for the UV-fluorescence, and that an increased particle size induces a shift from one mechanism to the other.

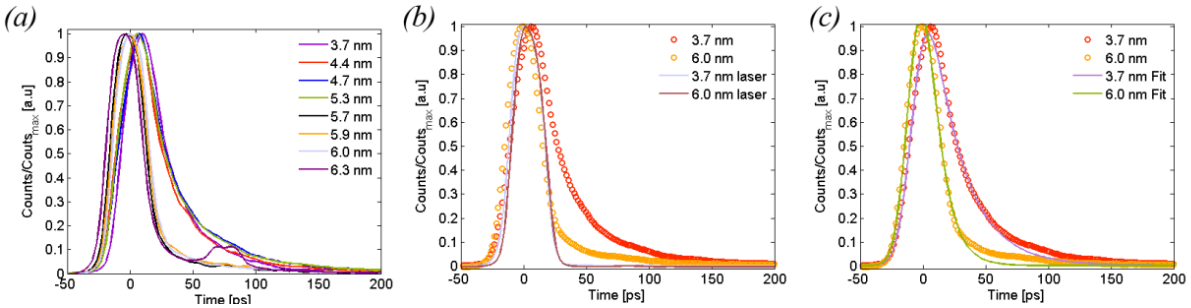

Figure 6. (a) Normalized time-track for the full sample set. The bump around 75 ps for the 6.3 nm sample is an effect of a laser artifact in the measurement. (b) Comparison of the time track for the laser pulse and the UV-decay for the 3.7 and 6.0 nm particles. Normalized data is used. (c) A single exponential fit to the experimental data.

If instead a two exponential decay is assumed and fitted to the experimental data, the trend is the same, even if the values change somewhat. The first, dominating exponent, shows a longer lifetime for the smaller particles and a shorter one for the larger particles. The second exponent has the opposite behavior but the amplitude is small, especially for the larger particles. It is thus doubtful if a model with two exponentials gives any additional information in further specifying the values of the lifetimes. Considering the extra parameters included in the two exponential fit and the low amplitude of the second exponential, we consider the single exponential decay as a realistic model for separation of the lifetimes in the experimental data. In either case, response functions of the lifetimes reveal two separable groups of lifetimes with a discontinuous size dependent shift between them.

Table 1. Summary of key data.

Sample number	Eg [eV]	d [nm]	UV_{max} [nm]	E at UV_{max} [eV]	ΔE [eV]	τ_1 [ps]
1	3.66	3.7	348	3.57	0.099	25.3
2	3.58	4.3	353	3.52	0.053	25.7
3	3.54	4.7	357	3.48	0.059	29.6
4	3.50	5.2	359	3.46	0.039	29.2
5	3.47	5.7	359	3.46	0.013	9.80
6	3.46	5.8	361	3.44	0.024	11.3
7	3.45	5.9	361	3.44	0.019	10.3
8	3.44	6.2	362	3.43	0.018	10.9

5. Discussion

A sketch of possible transitions occurring in the quantum dots related to the fluorescence is given in figure 7. In the subsequent discussion, numbers given for transitions are referring to that figure. The particles investigated here also display the frequently seen yellow/green fluorescence[25], but none of the other visible transitions sometimes reported in the literature. The absolute energetic positions of the band edges are known for these particles[29], and the positions of trap levels can thus be related to those. It is further known that the visible fluorescence observed in these particles is caused by a transition from a trap state located around 0.35 eV below the conduction band edge, down to a deep trap state in the band gap[25], as well as that surface defects are important for this transition[25, 39, 40].

The excitation wavelength of 320 nm used in these experiments correspond to a photon energy of 3.9 eV, causing a transition *(1)* leading to hot carriers in both the valence and the conduction band. A consequence of the more cluster like orbitals in the smaller particles is a suppression of the phonon vibrations. This was investigated for these ZnO quantum dots in a previous paper, where in particularly the TO-phonons bands were found to be suppressed[37]. This could potentially lead to a decrease in the interaction between the phonons and the photo-excited charge carriers, resulting in a slower cooling behavior of the hot electrons, which would be highly interesting.

The fluorescence data in figure 3 indicate a very small amount of fluorescence for energies larger than the band gap energy, thus indicating the thermalization of the hot carriers *(2)* to be faster than 10 ps. For the ZnO quantum dots here investigated, no sign of hot carrier emission is hence seen. In light of the fast decay rate of the observed emission, there is no indication of a phonon cooling bottleneck, at least not at room temperature, despite the experimental evidence of TO-phonon confinement in these systems.

Figure 5.b shows that the fluorescence maximum does not coincide with the band gap energy *(3)*, indicating a fast transition *(5)* down to states slightly below the conduction band edge, from where the UV-emission can occur. It should be pointed out that energy states given as straight lines in figure 7, all are distributions of states with a certain spread in energy. This, together with vibrations in the small crystals, is a mechanism behind peak broadening. The measured UV fluorescence *(7)* is thus caused by a transition from these states, slightly under the conduction band edge, to states close to the valence band edge, rather than directly between the band edges *(3)*. An equivalent possibility is a transition occurring from the conduction band edge to states slightly above the valence band edge, quickly populated by the thermalized holes.

Together with data previously measured for the visible fluorescence on these particles[25], it can be deduced that the transitions responsible for the UV-emission *(7)* and the visible emission *(9)* is not starting from the same set of energy states. The visible fluorescence *(9)* is caused by a transition from a trap state located 0.35 eV below the conduction band edge, down to a trap states in the band gap. If the UV emission would occur from the same set of states, the acceptor state would need to be a hot hole deeper down in the valence band, which is a less likely explanation.

It is known that the visible and the UV emission are two competing processes, and if the intensity of one is decreasing, the intensity of the other is often increased[18,30,31]. It is further known that surface defects are important for the visible fluorescence[25, 39, 40] and a decrease in the amount of defects, the total amount of surface[24], or a surface treatment can reduced the intensity of the visible fluorescence, while simultaneously increase the intensity of the UV emission[41]. Some authors actually use a high value of the UV to visible emission ration as a sign of high quality ZnO[30]. Other do, however, advocate more caution[18]. The visible fluorescence is further more a much slower process with a decay time in the µs regime[40].

The visible fluorescence tends to be the dominant transition, not counting radiation less transitions *(10)*, despite the fact that it is considerably slower than the UV-emission. This could be accounted for if either the transition down to the trap level *(4)* and *(8)* are fast, or the conduction band are depleted of holes capable of accepting the electron. Van Dijken et. al. have in a series of papers proposed a mechanism to account for the visible fluorescence that correlates well with our experimental data[42-45]. One of the defects known in ZnO is oxygen vacancies, $V_O^{\bullet}$, that could trap a hole in the valence band *(11)* and form a trapped hole, $V_O^{\bullet\bullet}$, to which an electron can be transferred giving rise to the visible emission *(8)*. If the trapping of the hole *(11)* is a fast process, that would correlate well with the experimental findings here. It could also account for the importance of the surface, as the oxygen vacancies tend to accumulate at the surface unless it is specially treated.

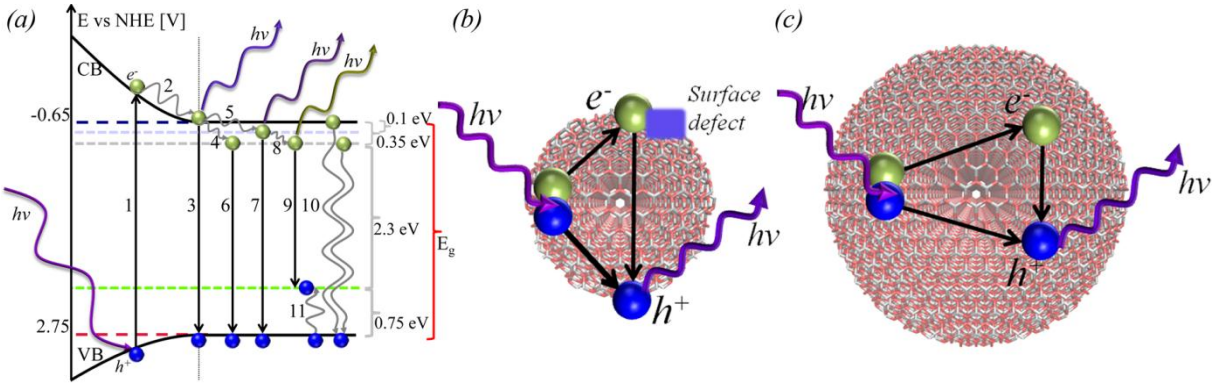

Figure 7. (a) Sketch of possible transition related to the UV-emission. (b) Illustration of more long lived UV-fluorescence for a smaller particle caused by a transition from an exciton stabilized by a surface defect. (c) Illustration of more short lived fluorescence in larger particles caused by exciton decay in the interior of the particle.

Left to explain is the discontinuous decay rate seen in figure 6. It is know that the change in the visible fluorescence in this size regime is a smooth and continuous function with respect to particle size. This indicates that the UV-transition in itself *(7)* is affected by the particle size.

A possible cause for a slower emission kinetics in smaller particles is the more cluster like orbitals. This leads to a lower orbital overlap, resulting in a smaller transition probability, which in turn translate into a slower decay rate. Such a mechanism would, however, cause a continuous shift in the decay rate with respect to particle size.

There are two theoretical papers from Fonoberov et. al.[41,46] that may spread some light over this behavior. They have theoretically distinguished different excitonic behavior in ZnO quantum dots: excitons confined within the particles and excitons bound to surface located acceptor state. According to their work, an exciton associated to an acceptor state at the surface would be slightly lower in energy, and would have a slower decay rate than an exciton confined in the interior of the particle. That correlates well with our experimental data, where the smallest particles have an UV-fluorescence corresponding to a smaller fraction of the band gap, as well as having a longer decay time. Our experimental data does thus support their theoretical model, but also reveals a discontinuous shift not predicted.

Fonoberov et al. also have one experimental paper[47] where photoluminescence spectroscopy is performed as a function of temperature on both 4 nm and 20 nm ZnO particles as well as on bulk ZnO. They found support for an acceptor bound exciton recombination for the smallest particles, whereas the larger particles were dominated by a confined exciton recombination, expect at lower temperatures. There are also a few other experimental papers discussing the

temperature dependence of the UV-fluorescence in different nanostructures, giving somewhat varied results[48-50].

The discontinuity in the decay time with particle size can be rationalized by a change of mechanism for the exciton recombination, where the exciton is bound to surface acceptor states on the smallest particles, whereas they are located in the bulk of the larger particles. This is illustrated in figure 7.b and 7.c. This transition is remarkably sharp, and in our case occurs between 5.3 and 5.7 nm in particle diameter. The exact size where this occurs will probably be affected to some extent by the synthesis procedure and the surface properties of the particles. It is, according to Fonoberovs paper[47], probably also a function of temperature. Light intensity can also have an effect for the overall fluorescence behavior; especially for high light intensities where defect states may be saturated and limit the extent of some of the transition, e.g. *(4)*. *(8)* and *(11)*.

6. Summary and conclusion

Ensembles of ZnO quantum dots of different particle sizes were deposited as thin films, on which the UV-fluorescence was measured with femtosecond laser spectroscopy. From the measurements, a blue shift in the fluorescence peak was observed with decreased particle size. The blue shift correlates with the band gap shift, whereas the difference in energy between the band gap and the fluorescence energy is larger for the smaller particles. For 3.7 nm particles, the fluorescence energy at the maximum is around 100 meV smaller than the band gap energy, whereas it deceases to around 20 meV for 6 nm particles. This could be compared to the ZnO exciton binding energy of 60 meV. It is known that the TO-phonons in ZnO quantum dots are suppressed, and the possibility of slowed hot carrier thermalization due to a phonon bottleneck is discussed. No verification of such a behavior could, however, be found within the response function of the detector system in the experiment. The hot carrier thermalization is thus bound to occur on a time scale faster than 10 ps.

While quantifying the decay kinetics, a discontinuity in the lifetime for the UV-fluorescence with respect to particle size was found. The lifetime for particles with diameters of 5.3 and below was found to be between 25 and 30 ps, whereas for larger particles it was around 10 ps. This indicates the presence of two different mechanisms for the UV-emission, depending on the particle size. The possible transitions for both the UV-transition and the visible transition, as well as their relation, are discussed in the light of the experimental findings. A possible explanation to the discontinuous life times is suggested, based on exciton surface trapping for the smallest particles. This experimentally confirms and extends the knowledge of theoretical predictions found in the literature concerning the UV-emission.

7. Supporting information

In the supporting information figures for the full sample set corresponding to figure 3.a, 3.b, 3.c and figure 6 are found. This material is available free of charge via the Internet at ……

8. Acknowledgment

We thank Ahmed El-Zohry and Erik Göransson for experimental help. We also thank the Knut and Alice Wallenberg Foundation for financial support

9. Referenses

1. C. Klingshirn, *Phys. Status Solidi B*, 2007, **244**, 3027-3073.
2. N. Serpone, D. Dondi and A. Albini, *Inorg. Chim. Acta*, 2007, **360**, 794-802.
3. S. Ekambaram, *J. Alloys Compd.*, 2005, **390**, L4-L6.
4. K. H. Brown, K. R. Wessells and S. Y. Hess, *International Journal for Vitamin and Nutrition Research*, 2007, **77**, 174-181.
5. G. Heideman, R. N. Datta, J. W. M. Noordermeer and B. van Baarle, *J. Appl. Polym. Sci.*, 2005, **95**, 1388-1404.
6. Z. K. Tang, G. K. L. Wong, P. Yu, M. Kawasaki, A. Ohtomo, H. Koinuma and Y. Segawa, *Appl. Phys. Lett.*, 1998, **72**, 3270-3272.
7. A. Tsukazaki, A. Ohtomo, T. Onuma, M. Ohtani, T. Makino, M. Sumiya, K. Ohtani, S. F. Chichibu, S. Fuke, Y. Segawa, H. Ohno, H. Koinuma and M. Kawasaki, *Nat. Mater*, 2005, **4**, 42-46.
8. C. J. Lee, T. J. Lee, S. C. Lyu, Y. Zhang, H. Ruh and H. J. Lee, *Appl. Phys. Lett.*, 2002, **81**, 3648-3650.
9. G. A. Zhu, R. S. Yang, S. H. Wang and Z. L. Wang, *Nano Lett.*, 2010, **10**, 3151-3155.
10. P. Sharma, A. Gupta, F. J. Owens, A. Inoue and K. V. Rao, *J. Magn. Magn. Mater.*, 2004, **282**, 115-121.
11. J. X. Wang, X. W. Sun, Y. Yang, H. Huang, Y. C. Lee, O. K. Tan and L. Vayssieres, *Nanotechnology*, 2006, **17**, 4995-4998.
12. M. A. Martinez, J. Herrero and M. T. Gutierrez, *Sol. Energy Mater. Sol. Cells*, 1997, **45**, 75-86.
13. Z. L. Wang, *Adv. Funct. Mater.*, 2008, **18**, 3553-3567.
14. X. Y. Xu, C. X. Xu, X. M. Wang, Y. Lin, J. Dai and J. G. Hu, *Crystengcomm*, 2013, **15**, 977-981.
15. M. Quintana, T. Edvinsson, A. Hagfeldt and G. Boschloo, *J. Phys. Chem. C*, 2007, **111**, 1035-1041.
16. T. J. Jacobsson and T. Edvinsson, *RSC Advances*, 2012, **2**, 10298-10305.
17. U. Ozgur, Y. I. Alivov, C. Liu, A. Teke, M. A. Reshchikov, S. Dogan, V. Avrutin, S. J. Cho and H. Morkoc, *J. Appl. Phys.*, 2005, **98**.
18. A. B. Djurisic and Y. H. Leung, *Small*, 2006, **2**, 944-961.
19. L. L. Han, L. Cui, W. H. Wang, J. L. Wang and X. W. Du, *Semicond. Sci. Technol.*, 2012, **27**.
20. S. Chawla, K. Jayanthi, S. Singh and H. Chander, *J. Cryst. Growth*, 2008, **310**, 3517-3521.
21. A. Asok, M. N. Gandhi and A. R. Kulkarni, *Nanoscale*, 2012, **4**, 4943-4946.
22. H. P. Wang, H. Jiang and X. M. Wang, *Chem. Commun.*, 2010, **46**, 6900-6902.
23. K. Matsuyama, K. Mishima, T. Kato and K. Irie, *J. Colloid Interface Sci.*, 2012, **367**, 171-177.
24. T. J. Jacobsson and T. Edvinsson, *Inorg. Chem.*, 2011, **50**, 9578-9586.
25. T. J. Jacobsson and T. Edvinsson, *J. Phys. Chem. C*, 2013, **117**, 5497-5504.
26. D. W. Bahnemann, C. Kormann and M. R. Hoffmann, *J. Phys. Chem.*, 1987, **91**, 3789-3798.
27. E. A. Meulenkamp, *J. Phys. Chem. B*, 1998, **102**, 5566-5572.
28. L. Spanhel and M. A. Anderson, *J. Am. Chem. Soc.*, 1991, **113**, 2826-2833.
29. T. J. Jacobsson and T. Edvinsson, *J. Phys. Chem. C*, 2012, **116**, 15692-15701.
30. Y. Kashiwaba, K. Haga, H. Watanabe, B. P. Zhang, Y. Segawa and K. Wakatsuki, *Phys. Status Solidi B*, 2002, **229**, 921-924.

31. X. Wang, S. Yang, J. Wang, M. Li, X. Jiang, G. Du, X. Liu and R. P. H. Chang, *Optical and Quantum Electronics*, 2002, **34**, 883-891.
32. A. J. Nozik, *Annu. Rev. Phys. Chem.*, 2001, **52**, 193-231.
33. A. J. Nozik, *Physica E-Low-Dimensional Systems & Nanostructures*, 2002, **14**, 115-120.
34. W. A. Tisdale, K. J. Williams, B. A. Timp, D. J. Norris, E. S. Aydil and X. Y. Zhu, *Science*, 2010, **328**, 1543-1547.
35. Y. Rosenwaks, M. C. Hanna, D. H. Levi, D. M. Szmyd, R. K. Ahrenkiel and A. J. Nozik, *Phys. Rev. B*, 1993, **48**, 14675-14678.
36. B. N. Murdin, W. Heiss, C. Langerak, S. C. Lee, I. Galbraith, G. Strasser, E. Gornik, M. Helm and C. R. Pidgeon, *Phys. Rev. B*, 1997, **55**, 5171-5176.
37. D. Raymand, T. J. Jacobsson, K. Hermansson and T. Edvinsson, *J. Phys. Chem. C*, 2012, **116**, 6893-6901.
38. H. F. McMurdie, M. C. Morris, E. H. Evans, B. Paretzkin and W. Wong-Ng, *Powder Diffr*, 1986, **1**, 40-43.
39. D. Li, Y. H. Leung, A. B. Djurisic, Z. T. Liu, M. H. Xie, S. L. Shi, S. J. Xu and W. K. Chan, *Appl. Phys. Lett.*, 2004, **85**, 1601-1603.
40. S. Monticone, R. Tufeu and A. V. Kanaev, *J. Phys. Chem. B*, 1998, **102**, 2854-2862.
41. V. A. Fonoberov and A. A. Balandin, *Appl. Phys. Lett.*, 2004, **85**, 5971-5973.
42. A. van Dijken, E. A. Meulenkamp, D. Vanmaekelbergh and A. Meijerink, *J. Lumin.*, 2000, **87-9**, 454-456.
43. A. van Dijken, E. A. Meulenkamp, D. Vanmaekelbergh and A. Meijerink, *J. Lumin.*, 2000, **90**, 123-128.
44. A. van Dijken, E. A. Meulenkamp, D. Vanmaekelbergh and A. Meijerink, *J. Phys. Chem. B*, 2000, **104**, 4355-4360.
45. A. van Dijken, E. A. Meulenkamp, D. Vanmaekelbergh and A. Meijerink, *J. Phys. Chem. B*, 2000, **104**, 1715-1723.
46. V. A. Fonoberov and A. A. Balandin, *Phys. Rev. B*, 2004, **70**.
47. V. A. Fonoberov, K. A. Alim, A. A. Balandin, F. X. Xiu and J. L. Liu, *Phys. Rev. B*, 2006, **73**.
48. H. C. Hsu, H. Y. Huang, M. O. Eriksson, T. F. Dai and P. O. Holtz, *Appl. Phys. Lett.*, 2013, **102**.
49. A. Chernikov, S. Horst, T. Waitz, M. Tiemann and S. Chatterjee, *J. Phys. Chem. C*, 2011, **115**, 1375-1379.
50. X. H. Zhang, S. J. Chua, A. M. Yong, S. Y. Chow, H. Y. Yang, S. P. Lau and S. F. Yu, *Appl. Phys. Lett.*, 2006, **88**.